Properties of Iron Primary Cosmic Rays
Results from the Alpha Magnetic Spectrometer
- SUPPLEMENTAL MATERIAL -

(AMS Collaboration)

For references see the main text.

Detector.— The tracker has nine layers, the first $L1$ at the top of the detector, the second $L2$ above the magnet, six $L3$ to $L8$ within the bore of the magnet, and the last $L9$ above the electromagnetic calorimeter. $L2$ to $L8$ constitute the inner tracker. Each layer of the tracker provides an independent measurement of the charge Z with a resolution of $\sigma_Z/Z = 3.0\%$ for iron nuclei. Overall, the inner tracker has a resolution of $\sigma_Z/Z = 1.3\%$. The spatial resolution in each tracker layer is 5.8 μm for iron nuclei [22]. Together, the tracker and the magnet measure the rigidity R of charged cosmic rays, with a maximum detectable rigidity of 3.5 TV for iron nuclei over the 3 m lever arm from $L1$ to $L9$. Figure S1 shows the AMS rigidity resolution $\Delta(1/R)$ as function of rigidity.

Two of the TOF planes are located above the magnet (upper TOF) and two planes are below the magnet (lower TOF). The overall velocity ($\beta = v/c$) resolution has been measured to be $\sigma(1/\beta) = 0.01$ for iron nuclei. This discriminates between upward- and downward-going particles. The pulse heights of the two upper planes are combined to provide an independent measurement of the charge with an accuracy $\sigma_Z/Z = 1.5\%$. The pulse heights from the two lower planes are combined to provide another independent charge measurement with the same accuracy.

Iron nuclei traversing AMS were triggered as described in Ref. [23].

Monte Carlo (MC) simulated events were produced using a dedicated program developed by the collaboration based on the GEANT4-10.3 package [24]. The program simulates electromagnetic and hadronic interactions of particles and nuclei in the material of AMS and generates detector responses.

Event Selection.— In the first 8.5 years AMS has collected 1.50×10^{11} cosmic ray events. The collection time used in this analysis includes only those seconds during which the detector was in normal operating conditions and, in addition, AMS was pointing within $40°$ of the local zenith and the ISS was outside of the South Atlantic Anomaly. Due to the geomagnetic field, this collection time increases with rigidity, reaching 1.98×10^8 s above 30 GV.

Iron events are required to be downward going and to have a reconstructed track in the inner tracker which passes through $L1$. In the highest rigidity region, $R \geq 1.2$ TV, the track is also required to pass through $L9$. Track fitting quality criteria such as a χ^2/d.o.f. < 10 in the bending coordinate are applied, similar to Ref. [23,26-27].

The measured rigidity is required to be greater than a factor of 1.2 times the maximum geomagnetic cutoff within the AMS field of view. The cutoff was calculated by backtracing [28] particles from the top of AMS out to 50 Earth's radii using the most recent International Geomagnetic Reference Field model [29].

Results of the further study of the "slab" model, Eq. (3)— For completeness, the fit results with Eq. (3) for the Fe/O flux ratio are listed in Table SA and shown in Fig. S8a.

Next, the ratio of the iron flux to the helium flux [34] was computed and is reported in Table SIII. The fit of Eq. (3) to the Fe/He flux ratio was performed and is shown in Fig. S8b. The fit results are listed in Table SA. As seen, the Δ parameter is compatible with zero, indicating that in the model the Fe/He flux ratio at the source is constant over the entire rigidity range.

As a further study we fit the high statistics He/O flux ratio from Ref. [34] to Eq. (3). The fit results are shown in Fig. S8c. The fit results are listed in Table SA. Note, that Δ is again consistent with zero.

Finally, to study the difference in the rigidity dependence of the Fe flux and the Ne, Mg,

and Si fluxes, the Fe/Si flux ratio was computed and is reported in Table SIV. The fit of Fe/Si flux ratio with Eq. (3) was performed and shown in Fig. S8d. The fit results are listed in Table SA. Contrary to other primary-to-primary ratios, the Fe/Si Δ value is different from zero (3σ). This shows that in this model the Fe and Si rigidity dependences at the source are different.

We observe that the model of Eq. (3) provides a good description of all AMS primary-to-primary flux ratios over the entire rigidity range. Note, that the λ parameter values are consistent between all AMS primary-to-primary flux ratios (see Table SA).

TABLE SA. Fit results with Eq. (3) for the Fe/O, Fe/He, He/O, and Fe/Si flux ratios. The (fit) errors take into account the statistical and systematic errors from the flux ratio. The (rig) errors are from varying the λ_S rigidity dependence within its uncertainties, see Eq. (4). The (sig) error is an additional error on λ due to uncertainty in the evaluation of nuclei inelastic cross sections, see Eq. (5).

Flux Ratio	k	Δ	λ [g $\cdot$ cm^{-2}]	χ^2/d.o.f.
Fe/O	0.203 ± 0.006(fit)±0.006(rig)	-0.002 ± 0.015(fit) ± 0.009(rig)	1.04 ± 0.07(fit) ± 0.07(rig) ± 0.04(sig)	22/43
Fe/He	0.0081 ± 0.0003(fit)±0.0003(rig)	-0.012 ± 0.014(fit)±0.002(rig)	1.05 ± 0.05(fit)±0.04(rig)±0.03(sig)	42/43
He/O	25.3 ± 0.1(fit)±0.05(rig)	0.004 ± 0.005(fit)±0.005(rig)	0.96 ± 0.04(fit)±0.03 (rig)±0.04(sig)	54/64
Fe/Si	1.07 ± 0.03(fit)±0.02(rig)	0.048 ± 0.016(fit)±0.005(rig)	0.89 ± 0.13(fit)±0.04(rig)±0.05(sig)	19/43

Results of the study of the "leaky box" model, Eq. (6)— We have fitted the Fe/O and Fe/Si flux ratios over the entire rigidity range using the "leaky box" model, $\frac{1+\lambda_S\,\tilde{\sigma}_{A'}}{1+\lambda_S\,\tilde{\sigma}_A}$, describing the propagation of primary nuclei through the interstellar medium [39] together with the source term $k\left(\frac{R}{192\text{GV}}\right)^{\Delta}$:

$$\frac{\Phi_A}{\Phi_{A'}} = k\left(\frac{R}{192\text{ GV}}\right)^{\Delta}\frac{1 + \lambda_S\,\tilde{\sigma}_{A'}}{1 + \lambda_S\,\tilde{\sigma}_A} \tag{6}$$

where k, Δ, λ_S, $\tilde{\sigma}_A$, and $\tilde{\sigma}_{A'}$ are the parameters discussed in Eqs. (3, 4, 5). The fit parameters are k, Δ, and λ. The fit of the AMS Fe/O flux ratio yields $k = 0.192\pm0.008$, $\Delta = 0.14\pm0.02$, and $\lambda = 0.57 \pm 0.11$ g cm^{-2} with χ^2/d.o.f.=155/43. The fit results are shown in Fig. S9a. The fit of the AMS Fe/Si flux ratio yields $k = 1.05 \pm 0.04$, $\Delta = 0.12 \pm 0.02$, and $\lambda = 0.49 \pm 0.15$ g cm^{-2} with χ^2/d.o.f.=66/43. The fit results are shown in Fig. S9b. As seen, Eq. (6) does not fit the AMS data.

TABLE SI: The Fe flux Φ as a function of rigidity at the top of AMS in units of $[\mathrm{m}^2 \cdot \mathrm{sr} \cdot \mathrm{s} \cdot \mathrm{GV}]^{-1}$ including errors due to statistics (stat.); contributions to the systematic error from the trigger and acceptance (acc.); the rigidity resolution function and unfolding (unf.); the absolute rigidity scale (scale); and the total systematic error (syst.). The contribution of individual sources to the systematic error are added in quadrature to arrive at the total systematic error.

Rigidity [GV]	Φ	$\sigma_{\text{stat.}}$	$\sigma_{\text{acc.}}$	$\sigma_{\text{unf.}}$	σ_{scale}	$\sigma_{\text{syst.}}$	
2.65 − 2.97	(9.354	0.087	0.425	0.379	0.015	0.570)	$\times 10^{-2}$
2.97 − 3.29	(8.392	0.066	0.371	0.228	0.006	0.436)	$\times 10^{-2}$
3.29 − 3.64	(7.459	0.053	0.324	0.148	0.001	0.356)	$\times 10^{-2}$
3.64 − 4.02	(6.577	0.045	0.281	0.104	0.004	0.300)	$\times 10^{-2}$
4.02 − 4.43	(5.898	0.038	0.250	0.078	0.006	0.262)	$\times 10^{-2}$
4.43 − 4.88	(5.088	0.031	0.214	0.057	0.007	0.221)	$\times 10^{-2}$
4.88 − 5.37	(4.387	0.025	0.183	0.043	0.007	0.188)	$\times 10^{-2}$
5.37 − 5.90	(3.810	0.022	0.159	0.032	0.007	0.162)	$\times 10^{-2}$
5.90 − 6.47	(3.260	0.019	0.136	0.024	0.007	0.138)	$\times 10^{-2}$
6.47 − 7.09	(2.798	0.016	0.116	0.019	0.006	0.118)	$\times 10^{-2}$
7.09 − 7.76	(2.333	0.013	0.097	0.015	0.006	0.098)	$\times 10^{-2}$
7.76 − 8.48	(1.967	0.011	0.082	0.012	0.005	0.083)	$\times 10^{-2}$
8.48 − 9.26	(1.662	0.009	0.069	0.009	0.004	0.070)	$\times 10^{-2}$
9.26 − 10.1	(1.398	0.008	0.058	0.008	0.004	0.059)	$\times 10^{-2}$
10.1 − 11.0	(1.173	0.007	0.049	0.006	0.003	0.049)	$\times 10^{-2}$
11.0 − 12.0	(9.879	0.064	0.411	0.049	0.030	0.415)	$\times 10^{-3}$
12.0 − 13.0	(8.147	0.058	0.340	0.038	0.025	0.343)	$\times 10^{-3}$
13.0 − 14.1	(6.982	0.051	0.292	0.031	0.022	0.294)	$\times 10^{-3}$
14.1 − 15.3	(5.747	0.045	0.241	0.025	0.019	0.242)	$\times 10^{-3}$
15.3 − 16.6	(4.817	0.039	0.202	0.020	0.016	0.204)	$\times 10^{-3}$
16.6 − 18.0	(4.077	0.034	0.171	0.016	0.014	0.173)	$\times 10^{-3}$
18.0 − 19.5	(3.355	0.030	0.141	0.012	0.012	0.142)	$\times 10^{-3}$
19.5 − 21.1	(2.842	0.026	0.120	0.010	0.010	0.121)	$\times 10^{-3}$
21.1 − 22.8	(2.372	0.022	0.100	0.008	0.009	0.101)	$\times 10^{-3}$
22.8 − 24.7	(1.962	0.018	0.083	0.006	0.007	0.084)	$\times 10^{-3}$
24.7 − 26.7	(1.651	0.016	0.070	0.005	0.006	0.070)	$\times 10^{-3}$
26.7 − 28.8	(1.403	0.014	0.059	0.004	0.005	0.060)	$\times 10^{-3}$
28.8 − 33.5	(1.072	0.010	0.044	0.003	0.004	0.045)	$\times 10^{-3}$
33.5 − 38.9	(7.235	0.075	0.300	0.018	0.028	0.302)	$\times 10^{-4}$
38.9 − 45.1	(5.066	0.058	0.210	0.011	0.020	0.211)	$\times 10^{-4}$
45.1 − 52.2	(3.433	0.045	0.143	0.007	0.014	0.143)	$\times 10^{-4}$
52.2 − 60.3	(2.485	0.036	0.103	0.005	0.010	0.104)	$\times 10^{-4}$
60.3 − 69.7	(1.723	0.028	0.072	0.004	0.008	0.072)	$\times 10^{-4}$
69.7 − 80.5	(1.186	0.021	0.049	0.002	0.005	0.050)	$\times 10^{-4}$
80.5 − 93.0	(8.141	0.164	0.339	0.018	0.039	0.342)	$\times 10^{-5}$
93.0 − 108	(5.490	0.123	0.229	0.013	0.028	0.231)	$\times 10^{-5}$
108 − 125	(3.625	0.094	0.152	0.010	0.020	0.153)	$\times 10^{-5}$
125 − 147	(2.397	0.067	0.101	0.007	0.014	0.102)	$\times 10^{-5}$

Table continued

Rigidity [GV]	Φ	$\sigma_{\text{stat.}}$	$\sigma_{\text{acc.}}$	$\sigma_{\text{unf.}}$	σ_{scale}	$\sigma_{\text{syst.}}$	
147 – 175	(1.516	0.047	0.064	0.005	0.010	0.065)	$\times 10^{-5}$
175 – 211	(9.926	0.335	0.420	0.042	0.072	0.428)	$\times 10^{-6}$
211 – 259	(5.897	0.224	0.251	0.029	0.049	0.257)	$\times 10^{-6}$
259 – 330	(3.364	0.139	0.144	0.019	0.033	0.149)	$\times 10^{-6}$
330 – 441	(1.568	0.076	0.068	0.011	0.020	0.071)	$\times 10^{-6}$
441 – 660	(6.567	0.350	0.288	0.060	0.120	0.318)	$\times 10^{-7}$
660 – 1200	(1.707	0.114	0.078	0.028	0.063	0.104)	$\times 10^{-7}$
1200 – 3000	(2.059	0.600	0.111	0.034	0.116	0.164)	$\times 10^{-8}$

TABLE SII: The iron to oxygen flux ratio Fe/O as a function of rigidity including errors due to statistics (stat.); contributions to the systematic error from the trigger, acceptance, and background (acc.); the rigidity resolution function and unfolding (unf.); the absolute rigidity scale (scale); and the total systematic error (syst.). The statistical errors are the sum in quadrature of the ratios of iron and oxygen flux statistical errors to the corresponding flux values, multiplied by the Fe/O flux ratio. The systematic errors from the background subtraction, the trigger, and the event reconstruction and selection are likewise added in quadrature. The correlations in the systematic errors from the uncertainty in nuclear interaction cross sections, the unfolding and the absolute rigidity scale between the iron and oxygen fluxes have been taken into account in calculating the corresponding systematic errors of the Fe/O flux ratio. The contribution of individual sources to the systematic error are added in quadrature to arrive at the total systematic uncertainty.

Rigidity [GV]	Fe/O	$\sigma_{\text{stat.}}$	$\sigma_{\text{acc.}}$	$\sigma_{\text{unf.}}$	σ_{scale}	$\sigma_{\text{syst.}}$
2.65 − 2.97	0.0699	0.0007	0.0024	0.0026	0.0000	0.0035
2.97 − 3.29	0.0708	0.0006	0.0024	0.0017	0.0000	0.0029
3.29 − 3.64	0.0721	0.0005	0.0023	0.0013	0.0000	0.0027
3.64 − 4.02	0.0737	0.0005	0.0024	0.0010	0.0000	0.0026
4.02 − 4.43	0.0776	0.0005	0.0024	0.0009	0.0000	0.0026
4.43 − 4.88	0.0789	0.0005	0.0025	0.0008	0.0000	0.0026
4.88 − 5.37	0.0809	0.0005	0.0025	0.0007	0.0000	0.0026
5.37 − 5.90	0.0842	0.0005	0.0026	0.0006	0.0000	0.0027
5.90 − 6.47	0.0865	0.0005	0.0027	0.0006	0.0000	0.0027
6.47 − 7.09	0.0896	0.0005	0.0028	0.0005	0.0000	0.0028
7.09 − 7.76	0.0907	0.0005	0.0028	0.0005	0.0000	0.0029
7.76 − 8.48	0.0928	0.0005	0.0029	0.0005	0.0000	0.0029
8.48 − 9.26	0.0955	0.0006	0.0030	0.0005	0.0000	0.0030
9.26 − 10.1	0.0980	0.0006	0.0031	0.0005	0.0000	0.0031
10.1 − 11.0	0.1006	0.0006	0.0031	0.0005	0.0000	0.0032
11.0 − 12.0	0.1034	0.0007	0.0032	0.0004	0.0000	0.0033
12.0 − 13.0	0.1038	0.0008	0.0033	0.0004	0.0000	0.0033
13.0 − 14.1	0.1083	0.0008	0.0034	0.0004	0.0000	0.0035
14.1 − 15.3	0.1089	0.0009	0.0035	0.0004	0.0000	0.0035
15.3 − 16.6	0.1108	0.0009	0.0035	0.0004	0.0000	0.0036
16.6 − 18.0	0.1148	0.0010	0.0037	0.0004	0.0000	0.0037
18.0 − 19.5	0.1148	0.0010	0.0037	0.0004	0.0000	0.0037
19.5 − 21.1	0.1186	0.0011	0.0038	0.0004	0.0000	0.0038
21.1 − 22.8	0.1205	0.0011	0.0039	0.0004	0.0000	0.0039
22.8 − 24.7	0.1220	0.0012	0.0040	0.0004	0.0000	0.0040
24.7 − 26.7	0.1257	0.0012	0.0041	0.0004	0.0000	0.0041
26.7 − 28.8	0.1304	0.0013	0.0043	0.0004	0.0000	0.0043
28.8 − 33.5	0.1325	0.0013	0.0042	0.0004	0.0000	0.0042
33.5 − 38.9	0.1323	0.0014	0.0042	0.0004	0.0000	0.0042
38.9 − 45.1	0.1373	0.0016	0.0044	0.0005	0.0001	0.0044
45.1 − 52.2	0.1362	0.0018	0.0044	0.0005	0.0001	0.0044
52.2 − 60.3	0.1452	0.0021	0.0047	0.0006	0.0001	0.0047

Table continued

TABLE SII – *(Continued)*.

Rigidity [GV]	Fe/O	$\sigma_{\text{stat.}}$	$\sigma_{\text{acc.}}$	$\sigma_{\text{unf.}}$	σ_{scale}	$\sigma_{\text{syst.}}$
60.3 − 69.7	0.1485	0.0024	0.0048	0.0006	0.0001	0.0049
69.7 − 80.5	0.1520	0.0028	0.0050	0.0007	0.0001	0.0050
80.5 − 93.0	0.1533	0.0031	0.0051	0.0007	0.0001	0.0051
93.0 − 108	0.1542	0.0035	0.0052	0.0007	0.0000	0.0052
108 − 125	0.1510	0.0040	0.0051	0.0007	0.0000	0.0052
125 − 147	0.1519	0.0043	0.0052	0.0008	0.0000	0.0053
147 − 175	0.1532	0.0048	0.0054	0.0008	0.0000	0.0054
175 − 211	0.1611	0.0055	0.0058	0.0009	0.0001	0.0058
211 − 259	0.1620	0.0063	0.0059	0.0011	0.0001	0.0060
259 − 330	0.1681	0.0071	0.0063	0.0014	0.0002	0.0065
330 − 441	0.1593	0.0078	0.0062	0.0017	0.0004	0.0064
441 − 660	0.1695	0.0092	0.0068	0.0027	0.0008	0.0074
660 − 1200	0.1565	0.0106	0.0067	0.0045	0.0008	0.0082
1200 − 3000	0.1369	0.0403	0.0076	0.0041	0.0007	0.0087

TABLE SIII: The iron to helium flux ratio Fe/He as a function of rigidity including errors due to statistics (stat.); contributions to the systematic error from the trigger, acceptance, and background (acc.); the rigidity resolution function and unfolding (unf.); the absolute rigidity scale (scale); and the total systematic error (syst.). The statistical errors are the sum in quadrature of the ratios of iron and helium flux statistical errors to the corresponding flux values, multiplied by the Fe/He flux ratio. The systematic errors from the background subtraction, the trigger, and the event reconstruction and selection are likewise added in quadrature. The correlations in the systematic errors from the uncertainty in nuclear interaction cross sections, the unfolding and the absolute rigidity scale between the iron and helium fluxes have been taken into account in calculating the corresponding systematic errors of the Fe/He flux ratio. The contribution of individual sources to the systematic error are added in quadrature to arrive at the total systematic uncertainty.

Rigidity [GV]	Fe/He	$\sigma_{stat.}$	$\sigma_{acc.}$	$\sigma_{unf.}$	σ_{scale}	$\sigma_{syst.}$	
2.65 − 2.97	(1.757	0.016	0.057	0.067	0.002	0.088)	$\times 10^{-3}$
2.97 − 3.29	(1.804	0.014	0.055	0.046	0.000	0.072)	$\times 10^{-3}$
3.29 − 3.64	(1.859	0.013	0.054	0.034	0.002	0.064)	$\times 10^{-3}$
3.64 − 4.02	(1.924	0.013	0.054	0.028	0.002	0.061)	$\times 10^{-3}$
4.02 − 4.43	(2.042	0.013	0.056	0.025	0.002	0.061)	$\times 10^{-3}$
4.43 − 4.88	(2.106	0.013	0.056	0.021	0.002	0.060)	$\times 10^{-3}$
4.88 − 5.37	(2.190	0.013	0.058	0.019	0.002	0.061)	$\times 10^{-3}$
5.37 − 5.90	(2.309	0.013	0.061	0.017	0.001	0.064)	$\times 10^{-3}$
5.90 − 6.47	(2.408	0.014	0.064	0.016	0.001	0.066)	$\times 10^{-3}$
6.47 − 7.09	(2.529	0.014	0.067	0.015	0.001	0.069)	$\times 10^{-3}$
7.09 − 7.76	(2.586	0.015	0.069	0.014	0.001	0.070)	$\times 10^{-3}$
7.76 − 8.48	(2.677	0.015	0.071	0.014	0.001	0.072)	$\times 10^{-3}$
8.48 − 9.26	(2.781	0.016	0.074	0.014	0.001	0.075)	$\times 10^{-3}$
9.26 − 10.1	(2.873	0.017	0.076	0.013	0.001	0.077)	$\times 10^{-3}$
10.1 − 11.0	(2.969	0.019	0.079	0.013	0.002	0.080)	$\times 10^{-3}$
11.0 − 12.0	(3.084	0.020	0.082	0.013	0.002	0.083)	$\times 10^{-3}$
12.0 − 13.0	(3.122	0.022	0.084	0.013	0.002	0.085)	$\times 10^{-3}$
13.0 − 14.1	(3.275	0.024	0.088	0.013	0.002	0.089)	$\times 10^{-3}$
14.1 − 15.3	(3.310	0.026	0.089	0.012	0.002	0.090)	$\times 10^{-3}$
15.3 − 16.6	(3.413	0.028	0.093	0.012	0.002	0.093)	$\times 10^{-3}$
16.6 − 18.0	(3.560	0.030	0.097	0.012	0.002	0.098)	$\times 10^{-3}$
18.0 − 19.5	(3.610	0.032	0.099	0.012	0.002	0.100)	$\times 10^{-3}$
19.5 − 21.1	(3.762	0.034	0.104	0.012	0.002	0.104)	$\times 10^{-3}$
21.1 − 22.8	(3.859	0.036	0.107	0.013	0.002	0.107)	$\times 10^{-3}$
22.8 − 24.7	(3.924	0.037	0.109	0.013	0.002	0.110)	$\times 10^{-3}$
24.7 − 26.7	(4.069	0.039	0.113	0.013	0.002	0.114)	$\times 10^{-3}$
26.7 − 28.8	(4.239	0.042	0.118	0.014	0.002	0.119)	$\times 10^{-3}$
28.8 − 33.5	(4.380	0.041	0.116	0.015	0.002	0.117)	$\times 10^{-3}$
33.5 − 38.9	(4.425	0.046	0.117	0.016	0.001	0.118)	$\times 10^{-3}$
38.9 − 45.1	(4.635	0.054	0.123	0.018	0.001	0.124)	$\times 10^{-3}$
45.1 − 52.2	(4.677	0.061	0.124	0.019	0.001	0.125)	$\times 10^{-3}$
52.2 − 60.3	(5.019	0.072	0.133	0.021	0.000	0.135)	$\times 10^{-3}$

Table continued

Rigidity [GV]	Fe/He	$\sigma_{\text{stat.}}$	$\sigma_{\text{acc.}}$	$\sigma_{\text{unf.}}$	σ_{scale}	$\sigma_{\text{syst.}}$	
60.3 − 69.7	(5.142	0.083	0.137	0.022	0.000	0.139)	$\times 10^{-3}$
69.7 − 80.5	(5.231	0.094	0.140	0.023	0.001	0.141)	$\times 10^{-3}$
80.5 − 93.0	(5.321	0.107	0.143	0.023	0.001	0.144)	$\times 10^{-3}$
93.0 − 108	(5.328	0.119	0.143	0.023	0.002	0.145)	$\times 10^{-3}$
108 − 125	(5.284	0.137	0.143	0.022	0.002	0.144)	$\times 10^{-3}$
125 − 147	(5.338	0.149	0.145	0.022	0.003	0.147)	$\times 10^{-3}$
147 − 175	(5.343	0.166	0.147	0.023	0.003	0.148)	$\times 10^{-3}$
175 − 211	(5.707	0.193	0.159	0.025	0.005	0.161)	$\times 10^{-3}$
211 − 259	(5.784	0.220	0.163	0.028	0.008	0.166)	$\times 10^{-3}$
259 − 330	(6.033	0.250	0.174	0.034	0.012	0.178)	$\times 10^{-3}$
330 − 441	(5.703	0.277	0.168	0.039	0.016	0.173)	$\times 10^{-3}$
441 − 660	(5.926	0.317	0.179	0.055	0.026	0.189)	$\times 10^{-3}$
660 − 1200	(5.660	0.379	0.177	0.091	0.059	0.207)	$\times 10^{-3}$
1200 − 3000	(4.662	1.358	0.200	0.136	0.038	0.245)	$\times 10^{-3}$

TABLE SIV: The iron to silicon flux ratio Fe/Si as a function of rigidity including errors due to statistics (stat.); contributions to the systematic error from the trigger, acceptance, and background (acc.); the rigidity resolution function and unfolding (unf.); the absolute rigidity scale (scale); and the total systematic error (syst.). The statistical errors are the sum in quadrature of the ratios of iron and silicon flux statistical errors to the corresponding flux values, multiplied by the Fe/Si flux ratio. The systematic errors from the background subtraction, the trigger, and the event reconstruction and selection are likewise added in quadrature. The correlations in the systematic errors from the uncertainty in nuclear interaction cross sections, the unfolding and the absolute rigidity scale between the iron and silicon fluxes have been taken into account in calculating the corresponding systematic errors of the Fe/He flux ratio. The contribution of individual sources to the systematic error are added in quadrature to arrive at the total systematic uncertainty.

Rigidity [GV]	Fe/Si	$\sigma_{\text{stat.}}$	$\sigma_{\text{acc.}}$	$\sigma_{\text{unf.}}$	σ_{scale}	$\sigma_{\text{syst.}}$
2.65 − 2.97	0.4990	0.0051	0.0181	0.0179	0.0001	0.0255
2.97 − 3.29	0.4988	0.0045	0.0177	0.0118	0.0000	0.0213
3.29 − 3.64	0.4980	0.0041	0.0175	0.0085	0.0000	0.0194
3.64 − 4.02	0.5050	0.0040	0.0176	0.0069	0.0000	0.0189
4.02 − 4.43	0.5261	0.0040	0.0182	0.0061	0.0000	0.0192
4.43 − 4.88	0.5254	0.0037	0.0181	0.0052	0.0000	0.0188
4.88 − 5.37	0.5385	0.0036	0.0185	0.0045	0.0000	0.0191
5.37 − 5.90	0.5558	0.0037	0.0191	0.0041	0.0000	0.0195
5.90 − 6.47	0.5629	0.0037	0.0194	0.0037	0.0000	0.0197
6.47 − 7.09	0.5784	0.0038	0.0199	0.0035	0.0000	0.0202
7.09 − 7.76	0.5760	0.0038	0.0198	0.0032	0.0000	0.0201
7.76 − 8.48	0.5933	0.0039	0.0205	0.0031	0.0000	0.0207
8.48 − 9.26	0.5997	0.0040	0.0207	0.0030	0.0000	0.0209
9.26 − 10.1	0.6119	0.0042	0.0212	0.0029	0.0000	0.0214
10.1 − 11.0	0.6226	0.0045	0.0216	0.0028	0.0000	0.0218
11.0 − 12.0	0.6409	0.0048	0.0223	0.0028	0.0001	0.0224
12.0 − 13.0	0.6406	0.0053	0.0223	0.0027	0.0001	0.0225
13.0 − 14.1	0.6607	0.0056	0.0231	0.0027	0.0001	0.0233
14.1 − 15.3	0.6641	0.0059	0.0233	0.0026	0.0001	0.0234
15.3 − 16.6	0.6753	0.0063	0.0238	0.0025	0.0001	0.0239
16.6 − 18.0	0.7012	0.0068	0.0247	0.0025	0.0001	0.0249
18.0 − 19.5	0.7019	0.0071	0.0248	0.0024	0.0001	0.0250
19.5 − 21.1	0.7184	0.0075	0.0255	0.0024	0.0002	0.0256
21.1 − 22.8	0.7356	0.0079	0.0262	0.0024	0.0002	0.0263
22.8 − 24.7	0.7403	0.0079	0.0264	0.0023	0.0002	0.0265
24.7 − 26.7	0.7573	0.0084	0.0271	0.0023	0.0002	0.0272
26.7 − 28.8	0.7740	0.0088	0.0278	0.0024	0.0002	0.0279
28.8 − 33.5	0.7901	0.0081	0.0275	0.0024	0.0002	0.0276
33.5 − 38.9	0.7807	0.0089	0.0272	0.0024	0.0002	0.0273
38.9 − 45.1	0.8075	0.0102	0.0282	0.0025	0.0003	0.0283
45.1 − 52.2	0.7918	0.0114	0.0278	0.0025	0.0003	0.0279
52.2 − 60.3	0.8536	0.0136	0.0300	0.0028	0.0003	0.0302

Table continued

TABLE SIV – *(Continued)*.

Rigidity [GV]	Fe/Si	$\sigma_{\text{stat.}}$	$\sigma_{\text{acc.}}$	$\sigma_{\text{unf.}}$	σ_{scale}	$\sigma_{\text{syst.}}$
60.3 — 69.7	0.8585	0.0152	0.0303	0.0030	0.0004	0.0305
69.7 — 80.5	0.8701	0.0173	0.0309	0.0031	0.0004	0.0311
80.5 — 93.0	0.8767	0.0196	0.0313	0.0033	0.0004	0.0314
93.0 — 108	0.8918	0.0221	0.0320	0.0034	0.0003	0.0322
108 — 125	0.8838	0.0253	0.0318	0.0035	0.0003	0.0320
125 — 147	0.9049	0.0280	0.0328	0.0038	0.0004	0.0330
147 — 175	0.8779	0.0302	0.0321	0.0039	0.0004	0.0323
175 — 211	0.9579	0.0361	0.0353	0.0048	0.0006	0.0357
211 — 259	0.9532	0.0404	0.0356	0.0055	0.0008	0.0360
259 — 330	1.0273	0.0477	0.0388	0.0071	0.0012	0.0395
330 — 441	0.9537	0.0515	0.0366	0.0085	0.0017	0.0376
441 — 660	1.0115	0.0606	0.0397	0.0134	0.0030	0.0420
660 — 1200	0.9840	0.0737	0.0399	0.0233	0.0031	0.0463
1200 — 3000	0.8840	0.2806	0.0474	0.0155	0.0010	0.0499
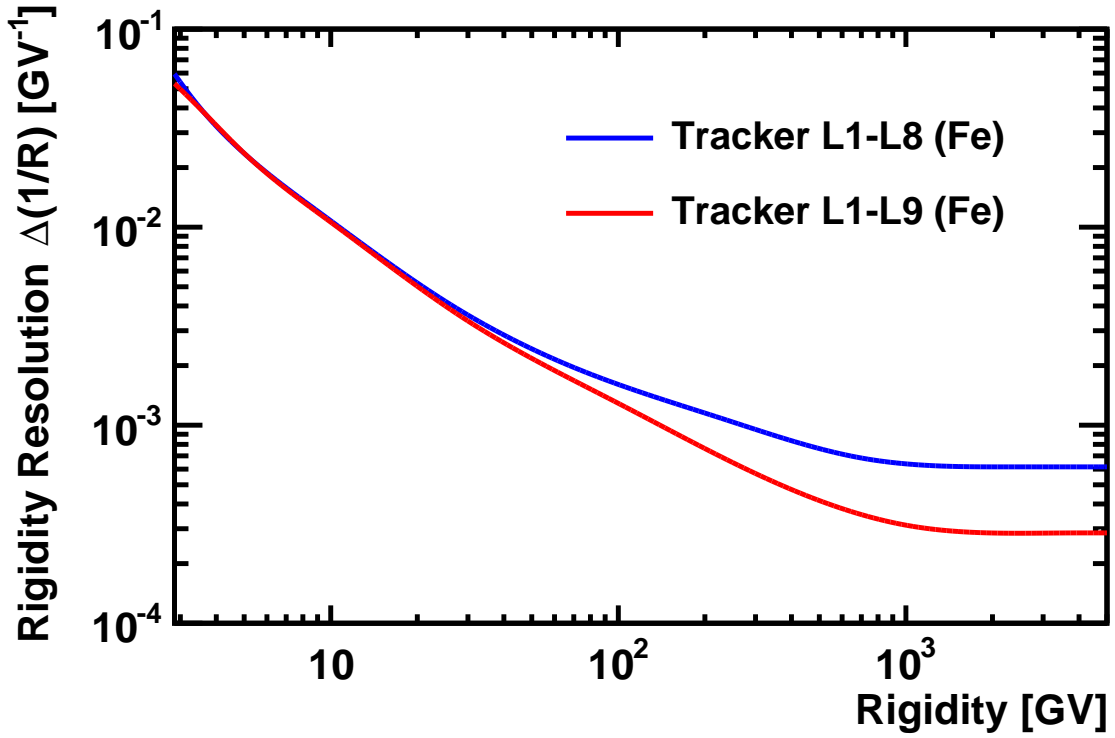
FIG. S1.   The AMS iron rigidity resolution as function of rigidity for two different configurations $L1$-$L8$ (blue curve) and $L1$-$L9$ (red curve).
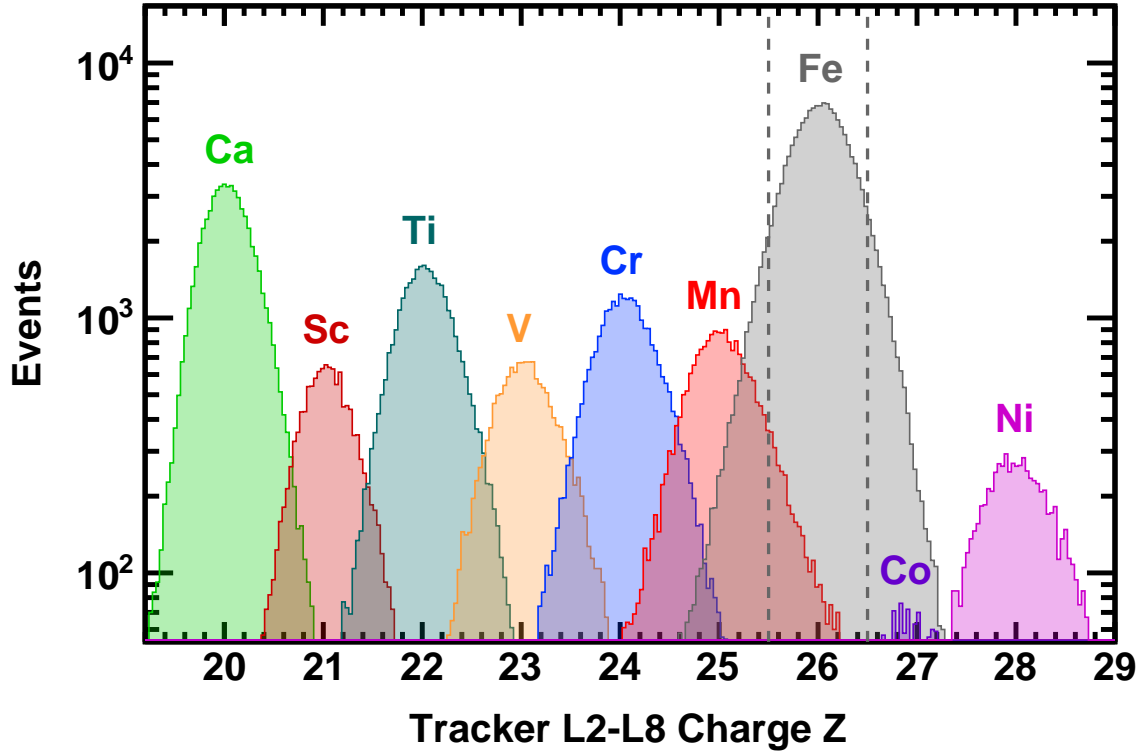
FIG. S2. Distribution of the charge measured with the inner tracker $L2$-$L8$ for samples from $Z = 20$ to $Z = 28$ selected by the tight cuts on charge measured with $L1$, the upper TOF, and the lower TOF over the rigidities above 4 GV. In particular, for Fe selection the following tight charge cuts on $L1$, the upper TOF, and the lower TOF were used: $24.8<Z_{L1}<26.5$, $25.5<Z_{UTOF}<26.5$, and $25.5<Z_{LTOF}<26.5$. The dashed vertical lines correspond to the charge selection in the inner tracker for iron, $25.5 < Z_{InnerTracker} < 26.5$.
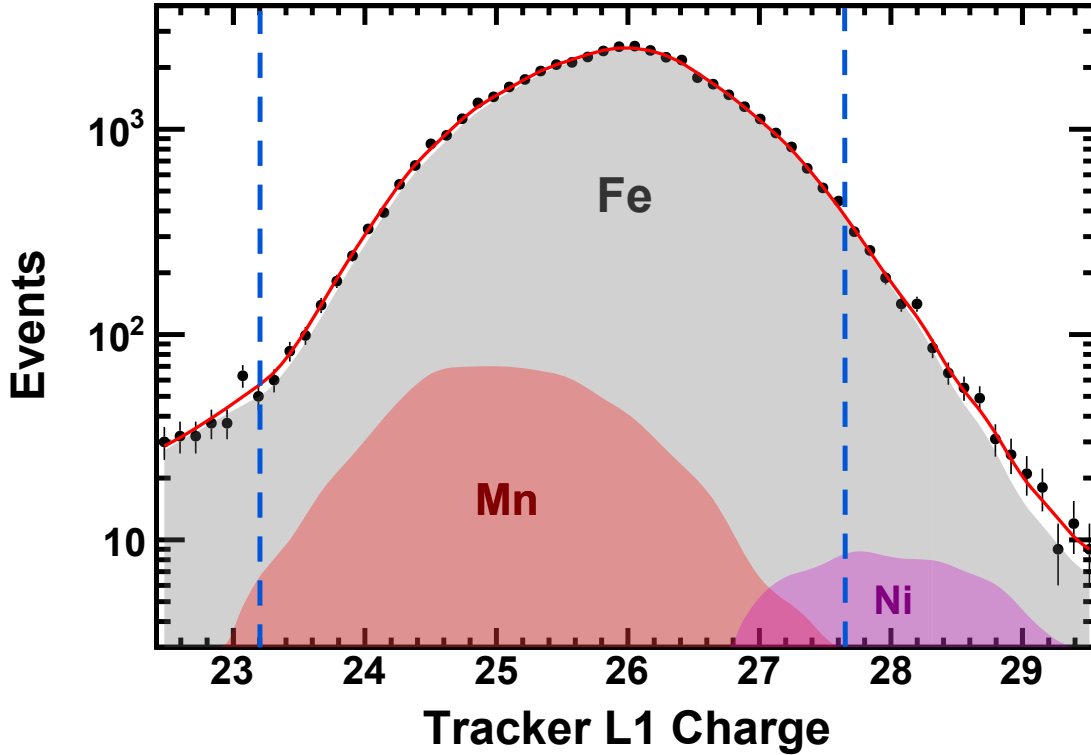
FIG. S3. Charge distributions measured by tracker $L1$ for iron events selected by the inner tracker $L2$-$L8$ in the rigidity range between 21 and 29 GV (black dots). The solid red curve shows the fit to the data of the sum of the Mn, Fe, and Ni charge distribution templates. The templates are obtained from non-interacting samples at $L2$ by using combined $L1$, upper TOF, $L3$-$L8$, and lower TOF charge selections. The charge selection applied on tracker $L1$ is shown as vertical dashed lines. As seen, the background from the $Z > 26$ nuclei is negligible ($< 0.3\%$).
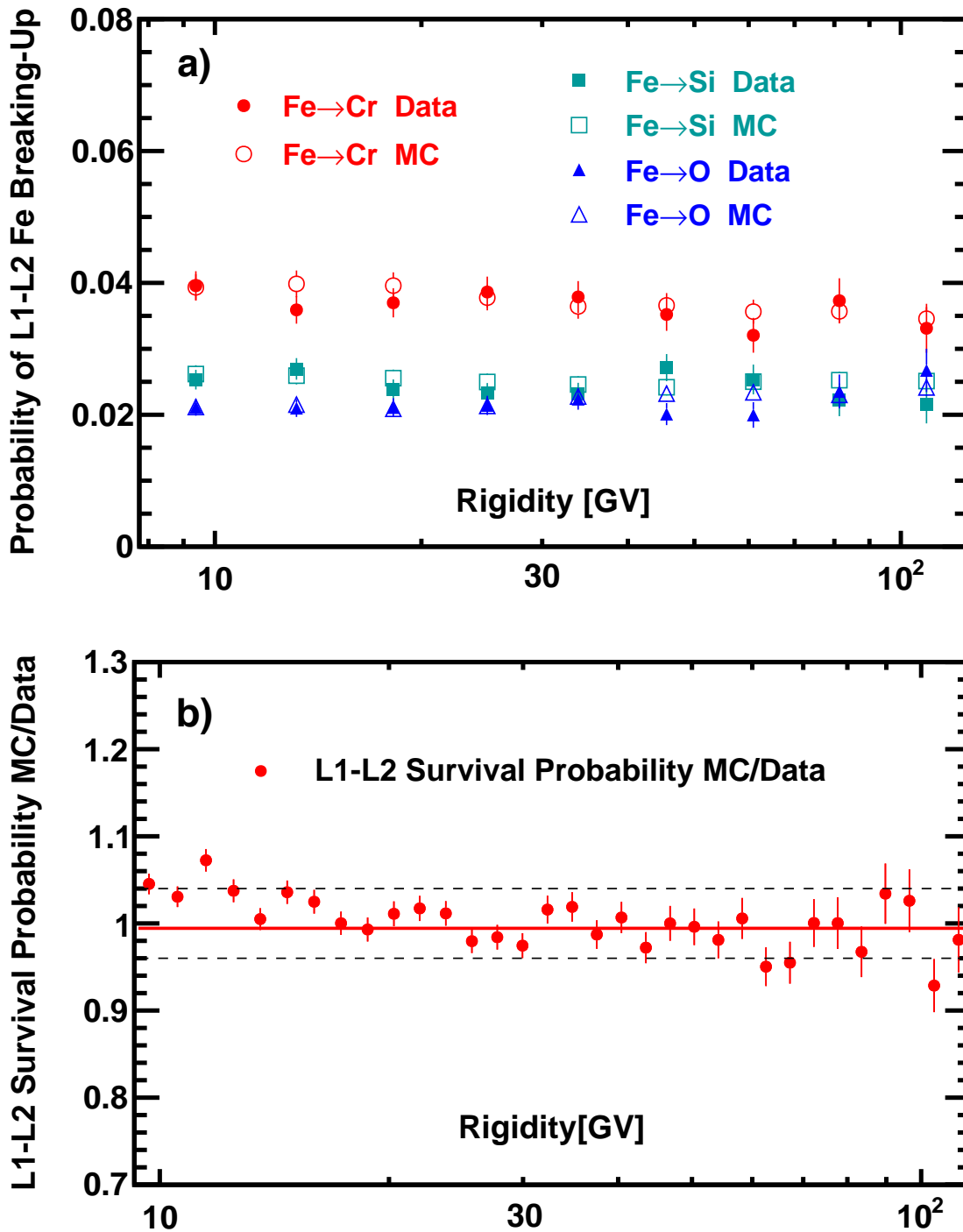
FIG. S4. a) Comparison of the simulated and measured Fe→Cr+X, Fe→Si+X, and Fe→O+X break-up probabilities between $L1$ and $L2$. b) The MC to data ratio of the iron survival probability between $L1$ and $L2$. The solid red line shows the average constant fit value and the black dashed lines indicate the estimated systematic error ranges (68% CL). The Fe survival probability between $L1$ and $L2$ is 45% for the rigidities above 4 GV.
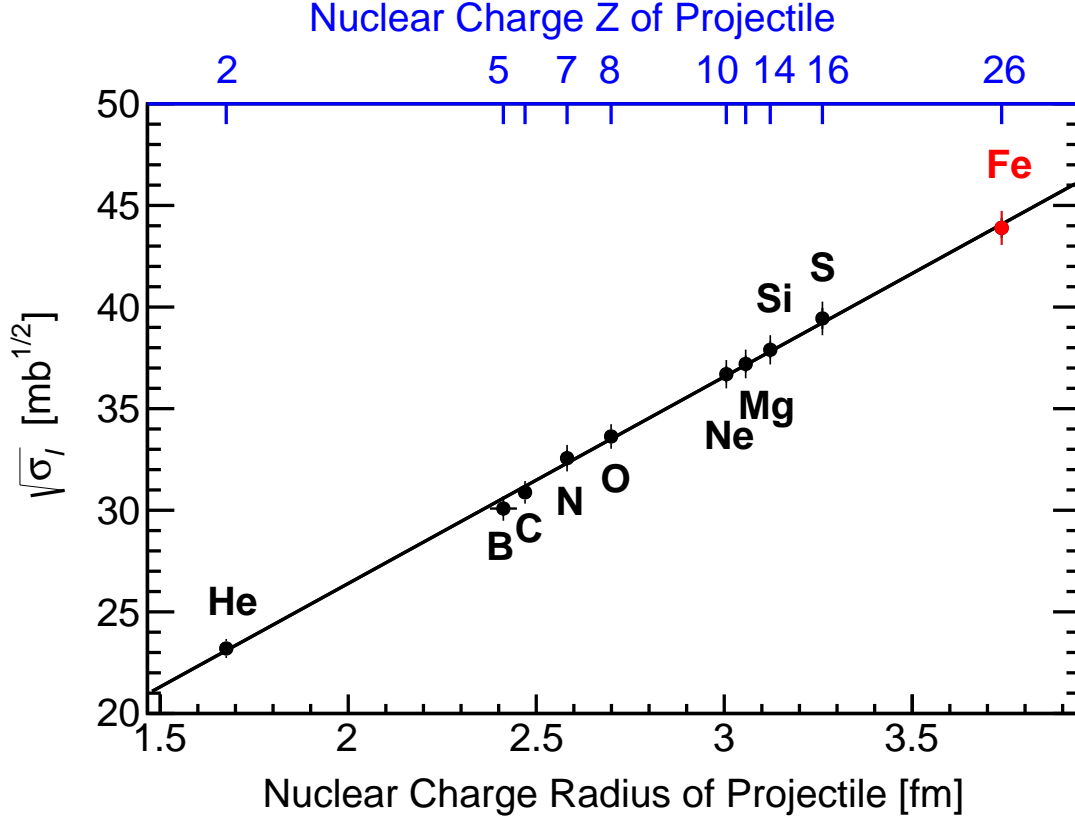
FIG. S5. The square root of the AMS measured interaction cross sections $\sqrt{\sigma_I}$ on a carbon target at rigidity 15 GV (black and red points) as a function of nuclear charge radius [31] for the projectile nuclei He, B, C, N, O, Ne, Mg, Si, and S from Ref. [30] and Fe from this Letter. The nuclei charge is indicated on the top scale. The solid black line shows the fit of $\sqrt{\sigma_I} = \kappa(r_P + r_T - r_0)$ [30], where κ is a geometrical factor, r_P is the projectile nuclei charge radius, r_T is the target (carbon) nuclei charge radius, and r_0 is an overlap parameter in the nuclear collision. The fit parameters are κ and r_0. The r_P and r_T are taken from Ref. [31]. The fit to the measured data yields $\kappa = 3.216 \pm 0.069(\text{fit}) \pm 0.047(\text{mat})$ and $r_0 = 1.875 \pm 0.070(\text{fit})$ fm with $\chi^2/\text{d.o.f.} = 2.9/8$, both parameters, κ and r_0, are consistent with Ref. [30]. The first error (fit) takes into account statistical and uncorrelated systematic errors, and the second error (mat) is the correlated error from the uncertainty on the AMS materials traversed by projectile nuclei [30].
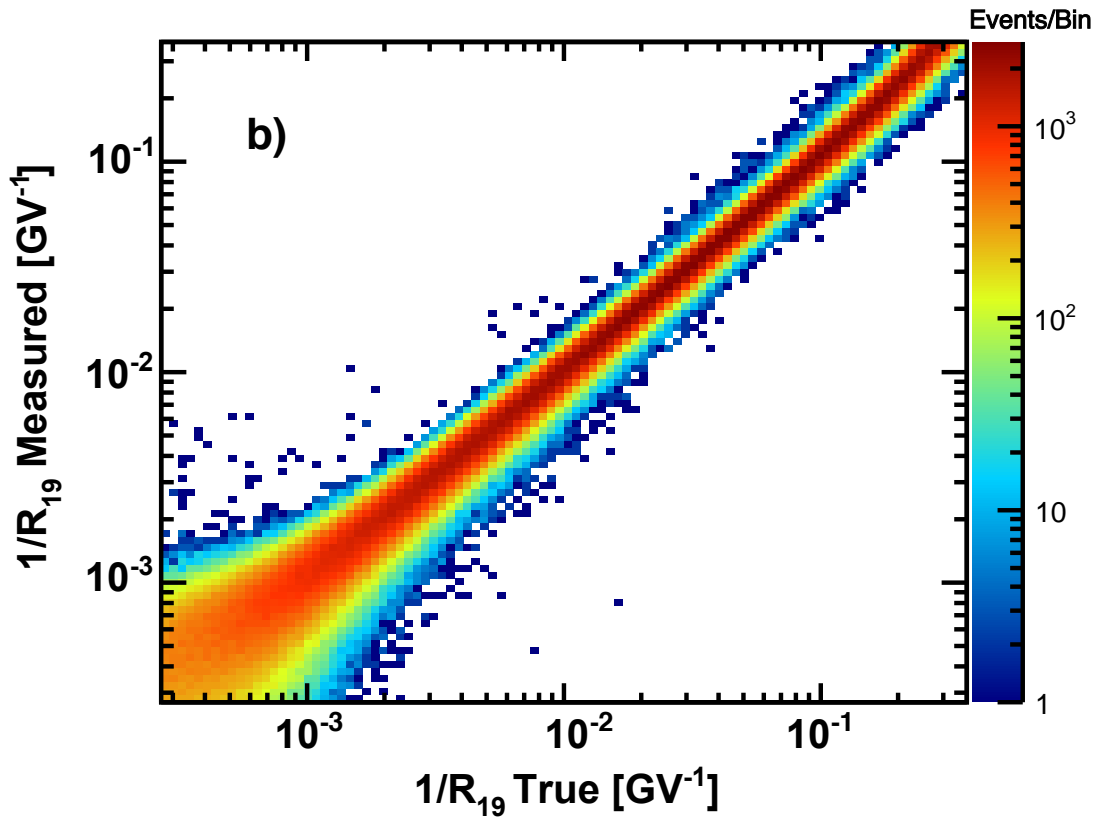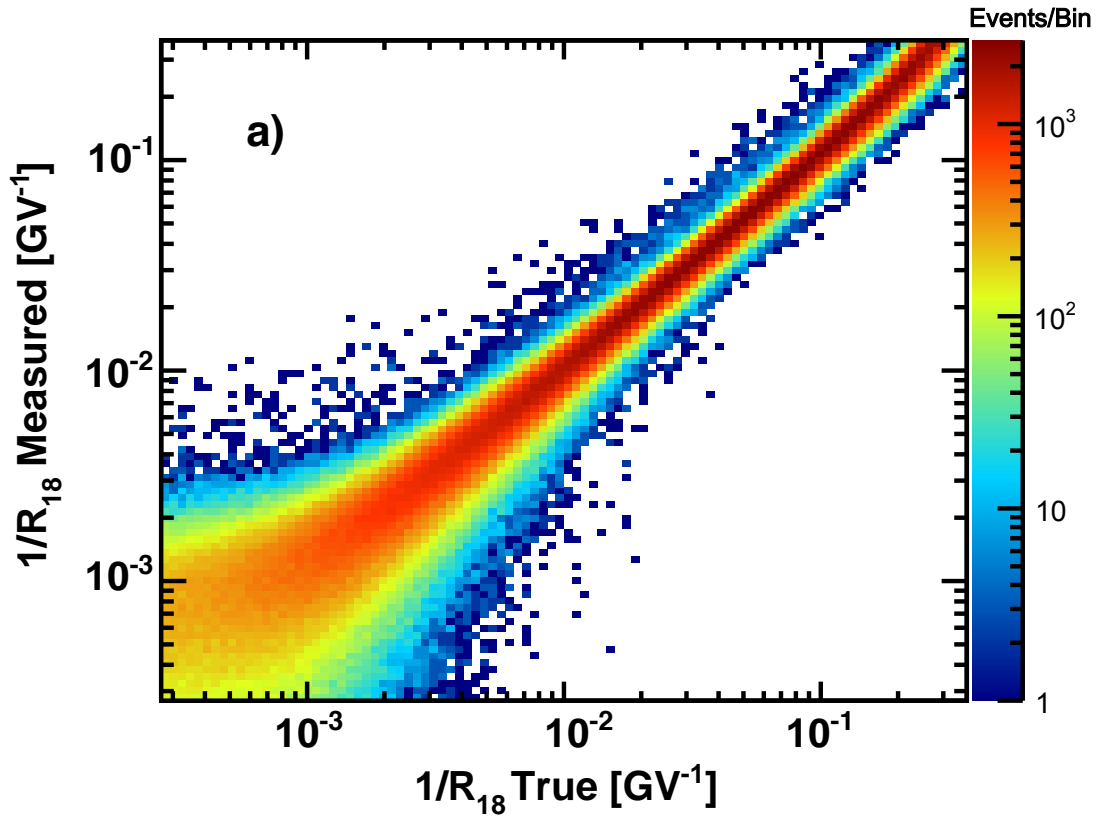
FIG. S6.   The AMS tracker rigidity resolution smearing matrices for the a) *L1-L8* and b) *L1-L9* configurations.
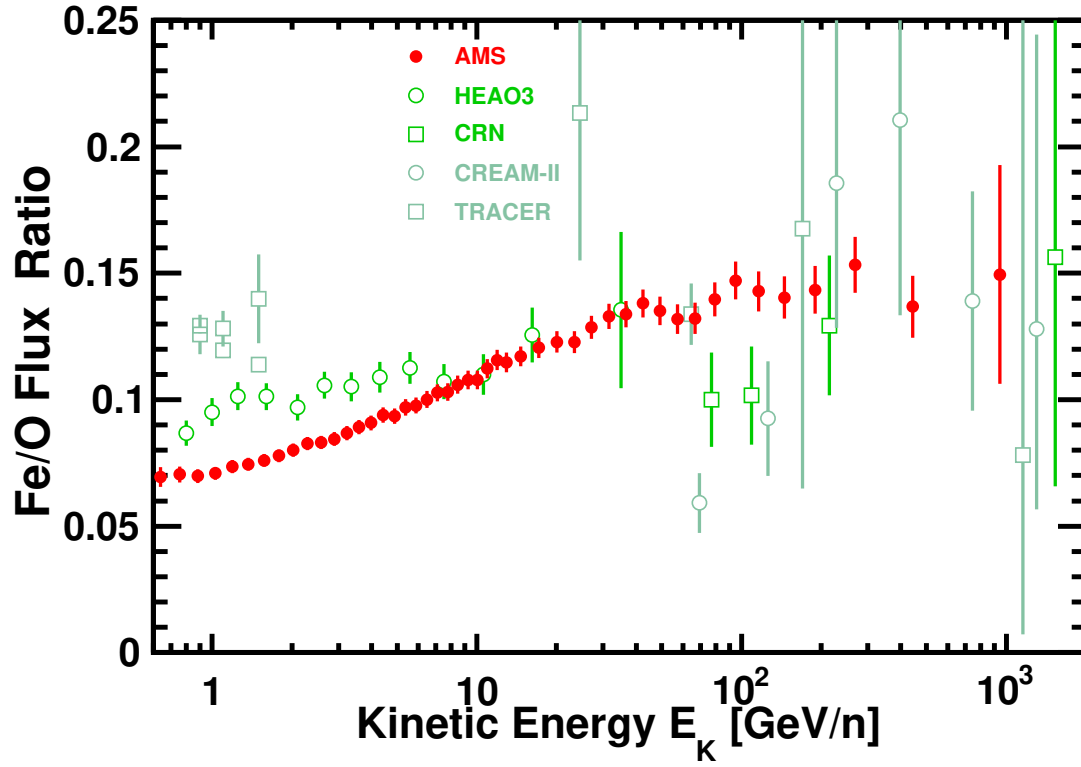
FIG. S7. The AMS Fe/O flux ratio as a function of kinetic energy per nucleon E_K together with earlier measurements. For the AMS measurements we used ^{56}Fe and ^{16}O.
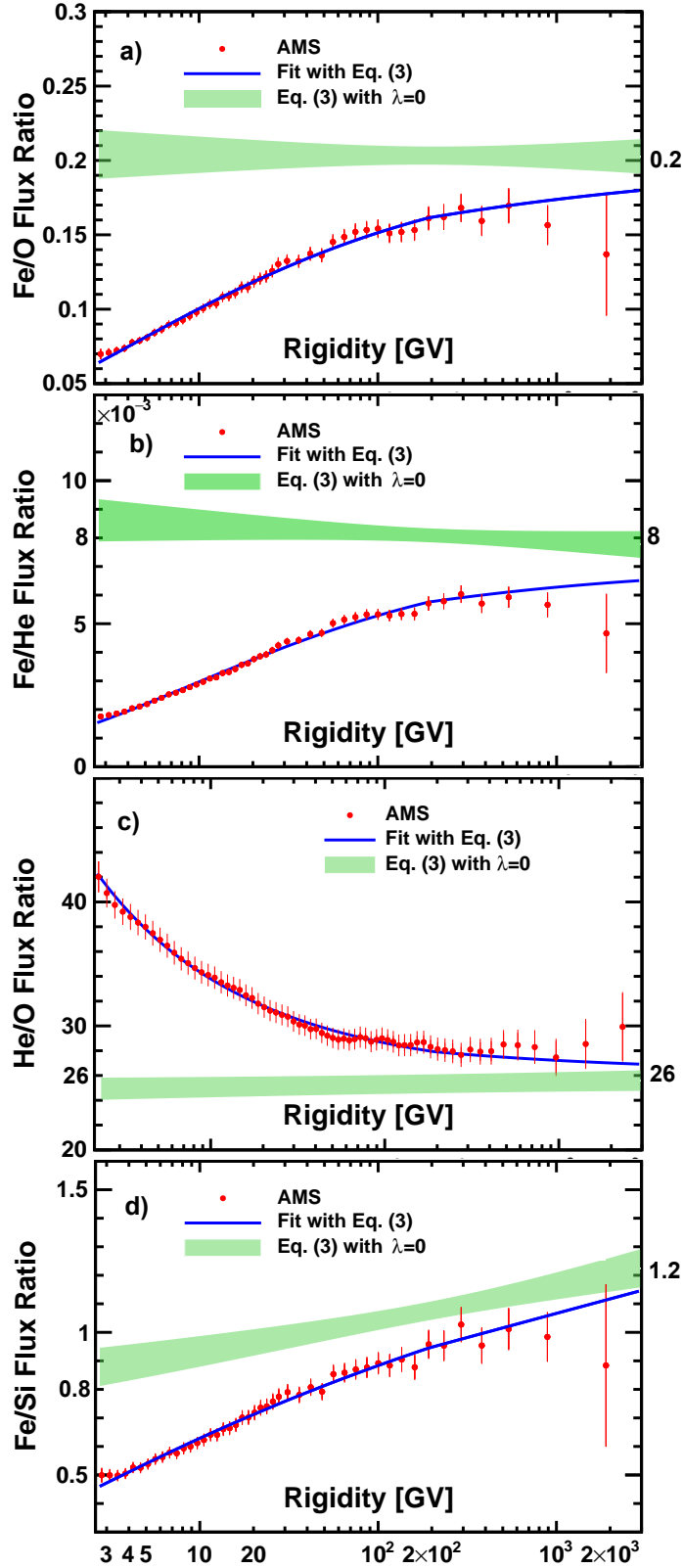
FIG. S8. The a) Fe/O, b) Fe/He, c) He/O, and d) Fe/Si flux ratios as a function of rigidity together with the fit of Eq. (3). The solid blue lines indicate the fit results. The green bands show the inferred flux ratios at the source, i.e. fit results of Eq. (3) with $\lambda = 0$. The band widths indicate the uncertainties (1σ). As seen, the Fe/O, Fe/He, and He/O flux ratios at the source are consistent with a constant over the entire rigidity range, whereas the Fe/Si flux ratio at the source is not constant at the 3σ level.
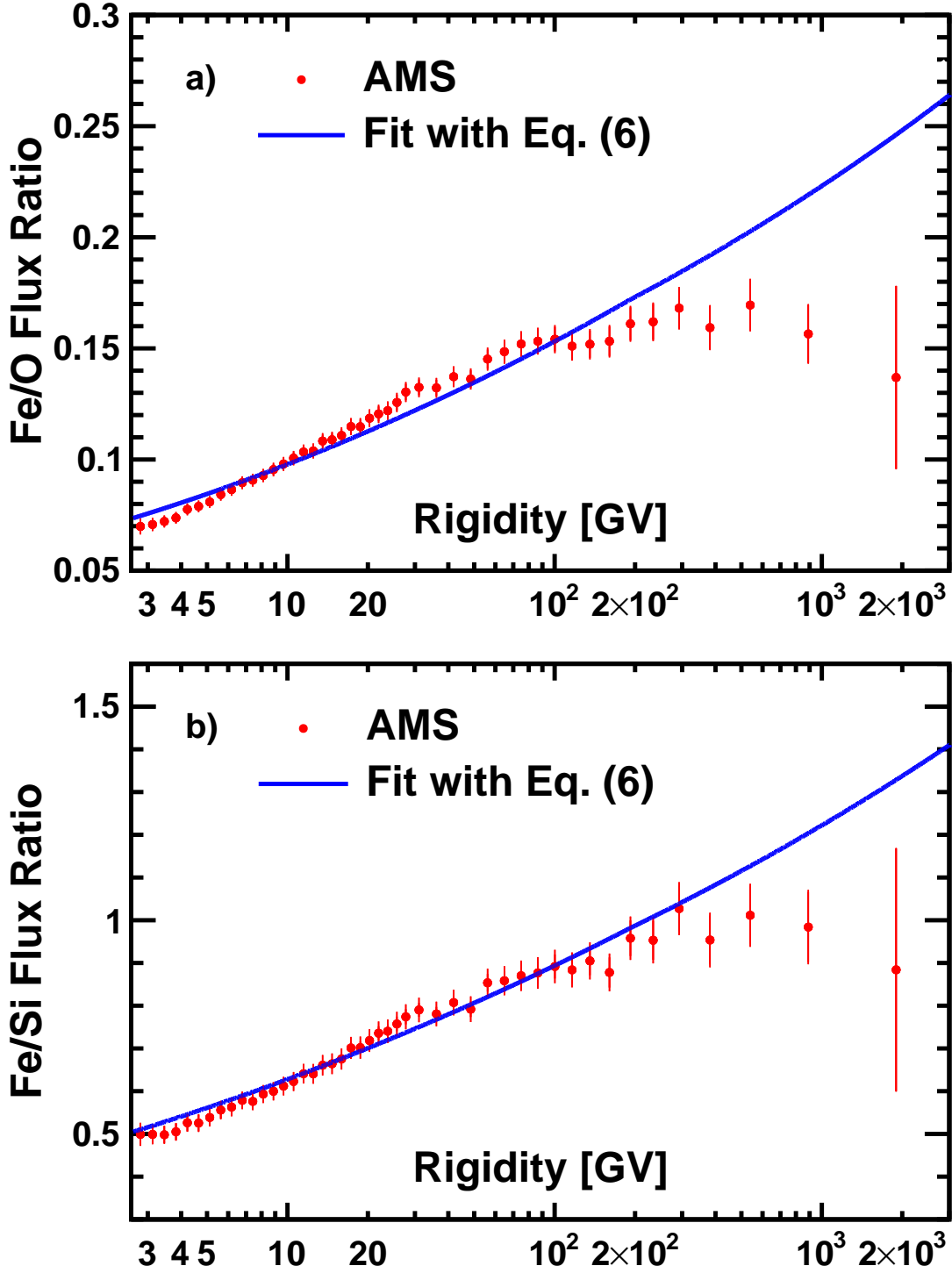
19

FIG. S9. The AMS a) Fe/O and b) Fe/Si flux ratio fit with Eq. (6). The solid blue lines indicate the fit results. As seen the "leaky box" model does not describe the AMS data.